Electron Transfer Triggers Fast Dimer/Monomer Switching of Pyridinium and Quinolinium Cations

ARTICLE *in* THE JOURNAL OF PHYSICAL CHEMISTRY C · JANUARY 2012

Impact Factor: 4.77 · DOI: 10.1021/jp211122n

7 AUTHORS, INCLUDING:

Filip Teplý
Academy of Sciences of the Czech Republic
59 PUBLICATIONS **1,433** CITATIONS
SEE PROFILE

Martina Čížková
Academy of Sciences of the Czech Republic
10 PUBLICATIONS **43** CITATIONS
SEE PROFILE

Viliam Kolivoska
Academy of Sciences of the Czech Republic
42 PUBLICATIONS **273** CITATIONS
SEE PROFILE

Magdaléna Hromadová
Academy of Sciences of the Czech Republic
84 PUBLICATIONS **830** CITATIONS
SEE PROFILE

THE JOURNAL OF PHYSICAL CHEMISTRY C

Article

pubs.acs.org/JPCC

Electron Transfer Triggers Fast Dimer/Monomer Switching of Pyridinium and Quinolinium Cations

Filip Teplý,[‡] Martina Čížková,[‡] Petr Slavíček,[§] Viliam Kolivoška,[†] Ján Tarábek,[‡] Magdaléna Hromadová,[†] and Lubomír Pospíšil*[,†,‡]

[†]J. Heyrovský Institute of Physical Chemistry of the ASCR, v.v.i., Dolejškova 3, 18223 Prague, Czech Republic

[‡]Institute of Organic Chemistry and Biochemistry of the ASCR, v.v.i., Flemingovo n. 2, 16610 Prague, Czech Republic

[§]Prague Institute of Chemical Technology, Technická 5, Prague 6, Czech Republic

Supporting Information

ABSTRACT: N-Heteroaromatic cations with quaternary pyridine-type nitrogen atoms have a rich application potential due to their bioactivity, fluorescence, and redox properties. Reactivity of radicals formed by reduction of such compounds is of key importance. We report the electron transfer mechanism of four novel compounds containing pyridinium, quinolinium, and benzothiazolium moiety. The reduction of pyridinium and quinolinium derivatives by one electron yields radicals that very rapidly form σ-dimers. Dimers can be converted to parent cations by oxidation, which proceeds at considerably higher potentials. Hence the dimerization can be reversibly switched by application of the appropriate electrode potential. In contrast, in benzothiazolium derivative the electron transfer yields a stable radical in which the follow-up dimerization reaction is completely blocked. Analysis of experimental data as well as theoretical models led to the identification of dimerization sites in reduced pyridinium and quinolinium species. We show the advantage of using the combination of electrochemical impedance data and simulation of cyclic voltammograms for estimation of kinetic parameters of the heterogeneous electron transfer rates and the coupled chemical reactions.

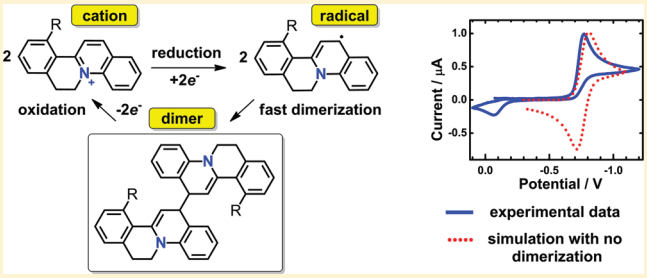

INTRODUCTION

Radicals of organic compounds play an important part in many natural[1,2] and synthetic[3−6] processes. Because of this central role of radicals in chemistry, properties and reactivity of electrogenerated free radicals are the subject of intensive current research efforts.[7−9] Radical−radical dimerization is the most commonly encountered reaction, which determines the lifetime of these very reactive species. The notion of this bimolecular reaction in the reduction of N-methylpyridinium salts dates back to 1956 when Majranovskij[10] described one-electron reduction of pyridinium cation, the redox potential of which shifts toward less negative values with increasing bulk concentration. The corresponding mechanism of the reduction of Ox to Red, followed by the dimerization to Dim

$$2\,\mathbf{Ox} + 2\,e^- \underset{}{\overset{k^0_{Red}}{\rightleftharpoons}} 2\,\mathbf{Red} \xrightarrow{k_{Dim}} \mathbf{Dim} \qquad (1)$$

was solved by Koutecký and Hanuš[11] and later applied by Blount and coworkers.[12] The theory of dimerization in cyclic voltammetry was developed by Olmstead,[13] and the diagnostic criteria for all different combinations of electrochemical and chemical reversibility were extensively worked out by the Savéant group.[14] In most cases, the chemical step is irreversible without any discernible dissociation because monomeric radicals recombine unpaired electrons yielding a σ−bonded dimer. One-way reductive dimerization of isoquinolinium system has been recently reported.[15] Reversible dimerization, which is a much less frequently observed phenomenon, is known to occur in several nitro- and cyano-substituted aromatic compounds.[16,17] Radicals can form still another type of adducts called π-dimers,[7−9,18,19] which exist in solutions and also in the solid state. The interaction of radicals with the parent redox form yields the precursor complex, which precedes the electron self-exchange.[20] These structures can be distinguished by characteristic absorption spectra.

Compounds selected for the present study contain quaternary nitrogen as a part of pyridinium (species **1**) or quinolinium moiety (species **2** and **3**). The structures are given in Chart 1. We will show that the reduction of these compounds initiates a very fast dimerization. Oxidation of the electrogenerated dimeric species triggers similarly fast dissociation of the dimers to recover the original monomeric form of compounds **1**−**3**. This cycle can be repeated. The series is supplemented by a related benzothiazolium derivative containing sulfur as an additional heteroatom (species **4**). Reduction of benzothiazolium **4** leads to formation of a stable radical, as

Received: November 18, 2011
Revised: January 3, 2012
Published: January 11, 2012

   dx.doi.org/10.1021/jp211122n | J. Phys. Chem. C 2012, 116, 3779−3786

Chart 1

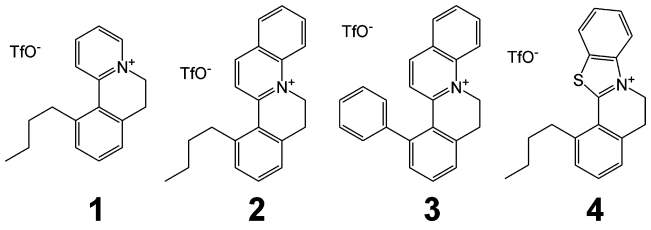

opposed to radicals with short lifetimes generated from pyridinium **1** and quinolinium **2** or **3**.

Preparation of compounds **1** to **4** was enabled by a flexible synthetic route to N-heteroaromatic cations based on [2 + 2 + 2] cycloaddition of cationic precursors, a strategy that was introduced recently by us.[21−24]

Specifically, the rapid synthetic assembly of cationic species **1** to **4** relied on three-step sequence of Sonogashira coupling, N-quaternization, followed by the key metal-catalyzed [2 + 2 + 2] cycloaddition of a cationic diyne with gaseous acetylene.[21]

The aim of this work is a detailed study of the kinetics of an electrochemically generated radicals and a reversible dimerization of compounds **1**−**3**. These compounds have been introduced as members of a novel family of readily available N-heteroaromatic cations with interesting potential uses as chemical probes for biology and as functional units for materials chemistry. We report the redox properties of the three compounds **1**−**3**, in which the dimerization process can be reversed upon electrochemical oxidation. Theoretical calculations are used to gain insight into the dimerization process and to identify the site at which the key bond formation occurs. Our study takes advantage of using the combination of voltammetric methods with the electrochemical impedance analysis, which is instrumental for reliable estimation of several kinetic processes involved in the overall mechanism. Nondimerizing benzothiazolium species **4** is investigated for comparison.

EXPERIMENTAL SECTION

Chemicals. The synthesis, purification, and full identification of all four compounds is described in our previous publication.[21]

Electrochemistry, Spectroelectrochemistry, and EPR Spectroscopy. Samples for electrochemical measurements were prepared in acetonitrile using 0.1 M tetrabutylammonium hexafluorophosphate ($TBAPF_6$) as the indifferent electrolyte. Acetonitrile was dried over activated molecular sieves, and $TBAPF_6$ was recrystallized and dried in vacuum. Electrochemical measurements were done using a system for DC polarography, cyclic voltammetry, phase-sensitive AC polarography, AC voltammetry, and electrochemical impedance spectroscopy (EIS). It consisted of a fast rise-time potentiostat, a lock-in amplifier (Stanford Research, model SRS830), and a frequency response analyzer (Stanford Research, model SRS760). The instruments were interfaced to a personal computer via an IEEE−interface card (PC-Lab, AdvanTech Model PCL-848) and a data acquisition card (PCL-818) using 12-bit precision for both A/D and D/A conversion. A three-electrode electrochemical cell was used. The reference electrode, Ag|AgCl|1 M LiCl, was separated from the test solution by a nonaqueous salt bridge. The potential of the ferrocene/ferrocenium redox couple (Fc/Fc^+) was 0.471 V. The working electrode was a computer-controlled valve-operated mercury drop (model SMDE2, Laboratorní přístroje, Prague). The auxiliary electrode was a platinum wire. The scan rate of the applied DC potential was in the range 0.05−50 V/s. Oxygen was removed from the solution by passing a stream of argon saturated with vapors of the solvent. Electrochemical experiments were performed at 25 ± 0.3 °C. The spectroelectrochemical data were obtained in an optically transparent thin-layer cell. The spectra were recorded using a diode-array UV−vis spectrometer from Agilent, model 8453 and a UV−vis-NIR spectrometer from Perkin-Elmer, Lambda 1050 model. The solutions of the cation radicals for the EPR spectroscopy were prepared by an exhaustive electrolysis in a cell with a separated compartment of the counter electrode and transferred under inert atmosphere to a flat quartz cuvette. The EPR spectra were recorded on EMXplus-10/12 CW (continuous wave) spectrometer (Bruker, Germany) equipped with the Premium X-band microwave bridge as well as with the high-sensitivity cavity E4119001 HS-W1 (Bruker, Germany). The determination of g factor was done using the built-in spectrometer frequency counter and the ER 036TM NMR-Teslameter (Bruker, Germany). The following parameters were set up to obtain the EPR spectra: the sweep width 40 mT, the resolution 4001 points, the microwave power 10 mW, the modulation amplitude 0.5 mT, the modulation frequency 100 kHz, the conversion time 25 ms, and the time constant 20.5 ms. To enhance the signal-to-noise ratio, we recorded the resulting spectrum as an accumulation of 40 individual spectra at the constant microwave frequency (f = 9.855397 GHz).

Calculation Methods. The electrochemical measurements were complemented by quantum chemical modeling. The calculations were performed to obtain (i) spin densities of the radical species, (ii) reduction potentials, and (iii) absorption spectra of the products formed upon the electrochemical reduction.

The spin densities were calculated at the density functional theory (DFT) level with B3LYP functional using 6-31 g* basis set. The SPARTAN (Jaguar 3.5, Schrödinger, Portland, OR) was used for these calculations. The quantitative characteristics (electrode potentials and absorption spectra) were calculated with BMK functional[25] containing 50% of HF exchange using 6-31+g* basis set. Electronically excited states were calculated with the time-dependent DFT (TDDFT) method. Gaussian 09 package[26] was used for all quantitative calculations.

DFT methods together with dielectric solvent models represent a reliable approach for modeling redox properties of organic molecules, in particular, one-electron redox potentials.[27] The redox potential E^0 for a redox couple

$$\mathrm{Ox(solv)} + \mathrm{e}^- \rightarrow \mathrm{Red(solv)} \quad (2)$$

is related to the free energies G^0 of the molecules in the oxidized and reduced forms via a relation

$$E^0 = G^0(\mathrm{Ox, solv}) - G^0(\mathrm{Red, solv}) - E^0(\mathrm{abs, ref}) \quad (3)$$

where E^0(abs, ref) is the absolute electrode potential of the reference electrode. The free energies, G^0, were calculated in the gas phase, and solvation energies estimated with the polarizable continuum model[28] (PCM) were then added. We have used the parametrization for acetonitrile implemented in the Gaussian09 package. The value of E^0(abs, ref) is typically considered to be 4.43 V for the normal hydrogen electrode in water solution.[29]

dx.doi.org/10.1021/jp211122n | J. Phys. Chem. C 2012, 116, 3779−3786

There are, however, two problems with the above protocol: first, it is inconsistent to compare experimental quantity (absolute electrode potential) with calculated values of free energies. Second, our measurements have been performed in acetonitrile solution, and the value of 4.43 V cannot be therefore directly applied. We have instead used a different protocol, calculating reduction potential against a standard with a well-defined reduction potential. Here we used indole as the standard (E^0 = 0.82 V vs Fc^+/Fc in acetonitrile[30]). We then calculated free-energy change ΔG^0 for a reaction

$$\mathrm{Ox(solv) + Ind(solv) \rightarrow Red(solv) + Ind^{\cdot +}(solv)} \quad (4)$$

where $\Delta G^0 = -F(E^0(\mathrm{Ox/Red}) - E^0(\mathrm{Ind^+/Ind}))$.

The absorption spectra were modeled via an empirical broadening scheme: the electronic transition quantities (oscillatory strengths and excitation energies) were calculated for the minimal geometries, and the spectra have been broadened with a predefined fwhm of 0.35 eV. We considered eight electronic states in our calculations; that is, only the spectrum above ~300 nm is captured. The software used for the simulation of cyclic voltammograms included DigiSim 3, version 3.03 (Bioanalytical Systems, USA) and ESP (http://lem.ch.unito.it/chemistry/electrochemistry.html, written by C. Nervi).

RESULTS AND DISCUSSION

DC Polarography and Cyclic Voltammetry. The first reduction of all four compounds proceeds as a seemingly simple reversible one-electron process yielding a single wave on the DC polarograms (Figure 1). The reduction potential of **1** is the most negative. The half-wave potentials are listed in Table 1 together with the log-plot slopes, which are close to the theoretical value 59 mV (2.303RT/F), suggesting the reversible character of the one-electron transfer. However, the cyclic voltammetry of compounds **1**−**3** indicates that a fast electron transfer is accompanied by a follow-up chemical step causing a chemical irreversibility. The voltammetric peak corresponding to the reduction does not have a corresponding counterpart (Figure 2A). A new oxidation peak is observed at considerably less negative potentials E_p^a, which are listed in Table 1.

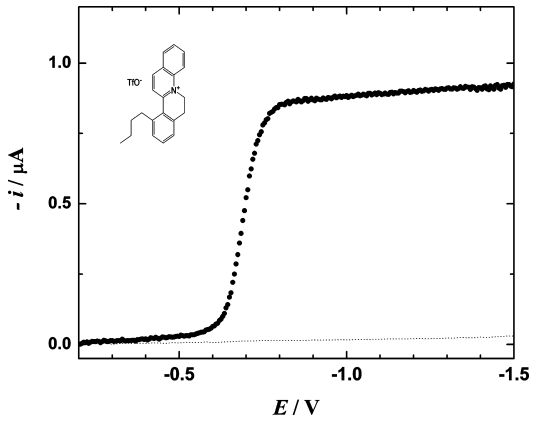

Figure 1. DC polarogram of 1.3 mM **2** in 0.1 M TBAFP6 in acetonitrile.

Table 1. Potentials of the Reduction, the Product Oxidation, and the Reversible Log-Plot Slopes from DC Polarography of 1 mM Solutions in Acetonitrile[a]

compound	$E_{1/2}$/V	log-plot slope/mV	E_p^a/V
1	−1.150	58	−0.61
2	−0.692	60	−0.07
3	−0.660	58	−0.12
4	−0.958	54	

[a]Ferrocene was +0.471 V.

The second voltage scan shows that the oxidation peak at E_p^a also lacks its reduction counter peak. Instead, the second scan yields almost identical reduction peak as that observed during the first voltage scan. The primary reduction product, a radical, undergoes a homogeneous reaction yielding a compound, which can be oxidized at E_p^a, thus restoring the original oxidized form. The initial estimate was that the chemical reaction is rather fast because the irreversibility of a voltammogram is still observed at the scan rate 100 V/s.

The benzothiazolium compound **4** behaves differently. The DC polarogram and also the cyclic voltammetry (Figure 2B) are in full agreement with a reversible one-electron transfer. There is no indication of a coupled homogeneous reaction. The origin of differences in behavior of the first three compounds **1**−**3** versus compound **4** was sought by application of spectroscopic and computation methods.

Spectroelectrochemistry and EPR Spectroscopy. The chemically reversible changes in the course of reduction−oxidation−reduction cycle of compounds **2** and **4** were confirmed by spectroelectrochemical data obtained in a thin layer cell. During the reduction of **2** at −1.2 V, the principal absorption band at 360 nm gradually decreases, and the fully reduced sample yields a weak band at 345 nm (Figure 3A). The reoxidation at 0.5 V restores the original absorption at 360 nm. These spectral changes are well-reproduced by quantum chemical calculations (Supplement 6 in the Supporting Information). The same reduction−oxidation cycle performed with **4** shows at −1.4 V a depletion of 340 nm absorbance, the appearance of a new band at 376 nm, and the restoration of the band at 340 nm by oxidation at 0 V (Figure 3B). Hence the spectroelectrochemistry confirms that the product of a chemical reaction can be reverted to the original form of **1**−**3**. Because the one-electron reduction of all four compounds yields a radical as a primary product, it is likely that the differences in radical reactions are responsible for a striking difference between reversibility of **4** and chemical irreversibility of other three derivatives. This is supported by EPR measurements of reduction products. The EPR signal yields only the reduced **4** (Figure 4), whereas reduction products of **1**−**3** are EPR silent. Analysis showed that the spectrum of the reduced **4** is centered at g_{iso} = 2.0156 with the ΔB_{pp}= 6.5 mT. The hyperfine splitting was not observed even at the lowest modulation amplitudes. This is evidently caused by a nonsymmetrical shape of the molecule and very small hyperfine splitting constants of hydrogen and nitrogen atoms.

Mechanism of Redox Reactions. Experimental results suggest that the chemical reaction following the electron transfer is a fast radical−radical dimerization, which is not observed in the case of **4**. Other types of subsequent chemical reactions leading to chemical irreversibility of the main voltammetric peak can be excluded. The disproportionation between primary radical product would yield also an EPR silent product. However, the reduction should consume two electrons, which is in disagreement with the wave height in Figure 1. Any kind of bond-breaking subsequent reactions

dx.doi.org/10.1021/jp211122n | J. Phys. Chem. C 2012, 116, 3779−3786

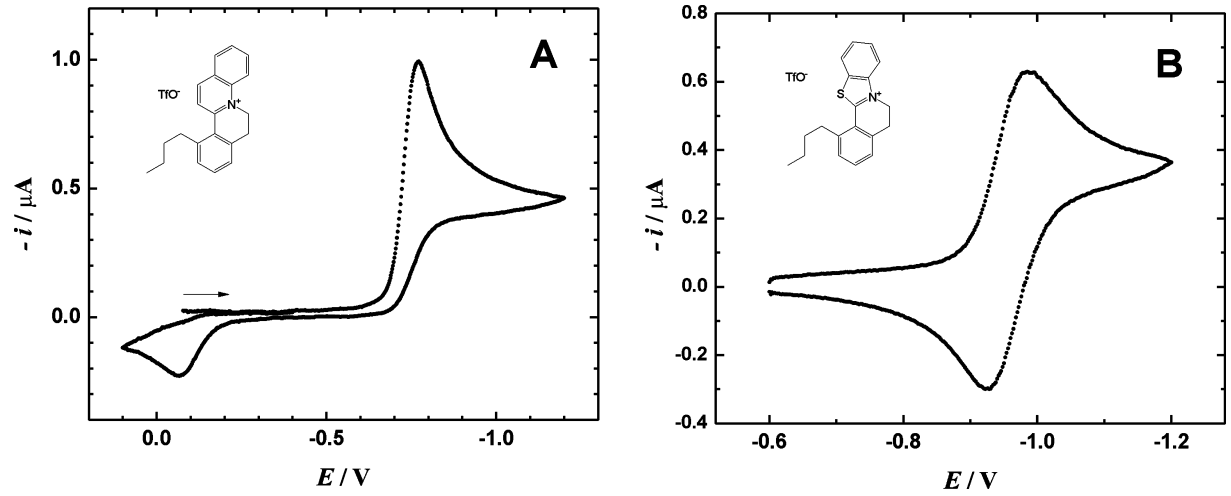

Figure 2. Cyclic voltammogram of (A) 1.3 mM **2** and (B) 0.53 mM **4** in 0.1 M TBAFP6 in acetonitrile. The scan rate was 62 mV/s. The arrow indicates the origin of the first voltage scan.

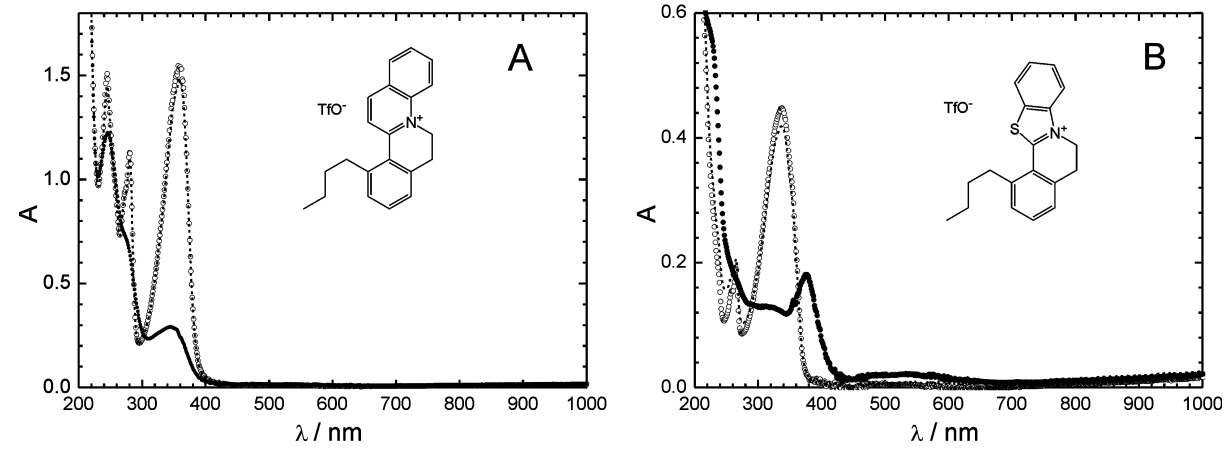

Figure 3. Spectroelectrochemistry of (A) 4.6 mM **2** and (B) 2 mM **4** during the reduction−oxidation cycle in a thin layer optical cell. Spectra correspond to the starting oxidized form (hollow points), to fully reduced form (full points), and to the reoxidized original form (dotted line).

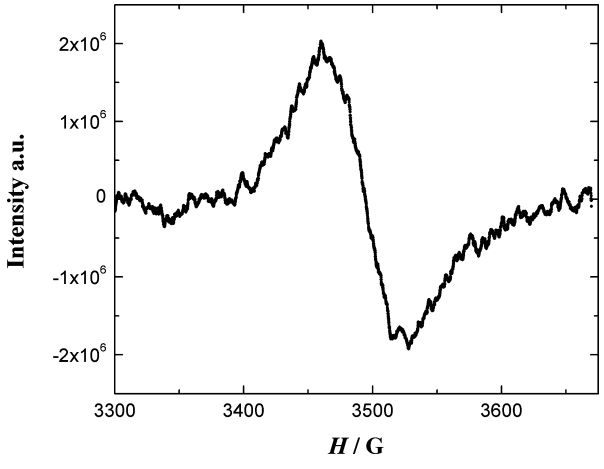

Figure 4. EPR spectrum of species obtained by electrochemical reduction of compound **4** at −1.25 V.

could also produce a new oxidation peak. The restoration of the main peak in the second voltage scan and the reversibility of spectral changes exclude such interpretation. For these reasons, the dimerization is the most plausible explanation. In such cases, the polarographic half-wave potential $E_{1/2}$ of compounds **1** to **3** should slightly depend on the bulk concentration of the oxidized form, thus reflecting the bimolecular type of the follow-up chemical reaction. Indeed, Figure 5 shows such dependence. The $E_{1/2}$ shifts by 28 ± 4 mV per one decade of concentration. Theoretically predicted change is 19 mV/decade; however, experimental values are often higher.[12] The peak potential E_{ac} of the AC polarograms shifts in a similar manner (Supplement 1 in the Supporting Information). The difference between E_{ac} and $E_{1/2}$ reflects a finite, although fast, charge transfer rate discussed below. Presented results are consistent with reduction of **4** proceeding according to a simple scheme

$$\mathbf{4}^{+} + e^{-} \leftrightarrows \mathbf{4}^{\cdot} \qquad (5)$$

yielding reversible DC polarograms, cyclic voltammograms, and also EPR signal of the radical.

The reduction of all compounds **1**−**3** involves a subsequent fast formation of a dimer, which is oxidized at considerably higher potentials to a product decomposing instantly to the original monomeric form. Using the notation $\mathbf{A}^{+}$ for cationic

dx.doi.org/10.1021/jp211122n | J. Phys. Chem. C 2012, 116, 3779−3786

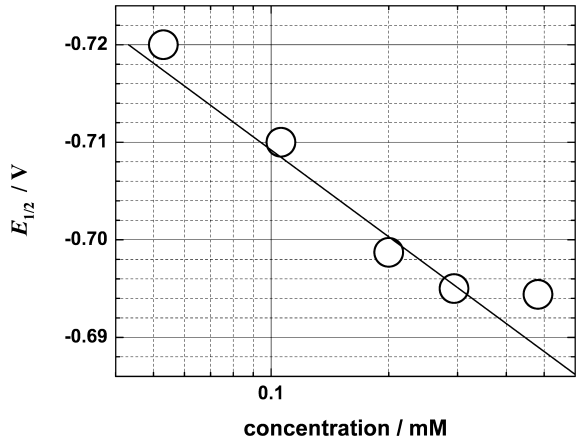

Figure 5. Shift of the redox potential with the bulk concentration evaluated from DC polarograms of **2** (hollow points). Line with the slope 28 mV/decade was obtained by the linear regression.

portion of all compounds **1**−**3** we can express the mechanism as follows

$$\begin{array}{ccc} 2\,\mathbf{A}^{+} + 2\,e^{-} & \xrightarrow{k^{0}_{Red}} & 2\,\mathbf{A}^{\bullet} \\ k_{Dis}\uparrow & & \downarrow k_{Dim} \\ {}^{+}\mathbf{A}\text{-}\mathbf{A}^{+} - 2\,e^{-} & \xleftarrow[k^{0}_{Ox}]{} & \mathbf{A}\text{-}\mathbf{A} \end{array} \qquad (6)$$

The heterogeneous rate constants are k^0, whereas k_{Dim} and k_{Dis} denote the homogeneous dimerization and dissociation rate constants, respectively. The potentials of $\mathbf{A}^+$ reduction and **A-A** oxidation differ by 0.5 V or more. (See Table 1.) The dissociation rate of **A-A** is negligibly low because the voltammetric oxidation peak of the $\mathbf{A}^{\bullet}$ was not observed at voltage sweep rates from 0.065 to 100 V/s. The dissociation rate of ${}^{+}\mathbf{A}\text{-}\mathbf{A}^{+}$ is very fast, and no reduction current on the third half-cycle is detectable at 100 V/s. For these reasons, we will not consider the back reactions of the two chemical steps in the mechanism. The estimation of kinetic parameters in eq 6 from voltammetric data is not a trivial task because there are too many unknown parameters. Hence an independent estimation of at least the electron transfer rate constants is desirable.

For this purpose, we applied the phase-sensitive AC polarography and the EIS in a broad range of frequencies. However, from AC data, another complicating factor, a weak but distinct adsorption of reactant, emerges. The theory for the faradaic impedance for a reversible electrodimerization has been worked out and applied by Rueda,[31] who also noticed adsorption complications, although with simpler compounds. However, the present case is unidirectional chemical reaction, which follows the electron transfer and is coupled to the adsorption. Therefore, we had to use an alternative approach.

The phase-sensitive AC polarography of **1** shows an asymmetrical imaginary faradaic maximum Y_F'' with a shoulder at −1.1 V (Figure 6A). The shoulder becomes still more noticeable at higher frequencies. The values of Y'' do not merge to the baseline, which is another indication of the reactant adsorption. Other derivatives **2** and **3** having an additional condensed aromatic ring show the adsorptive behavior still more clearly. The phase-sensitive AC polarography of **2** in acetonitrile (Figure 6B) shows a gradual increase in the imaginary admittance Y'' component with the bulk concentration at potentials on both sides of the admittance faradaic maximum Y_F''. Curves Y'' do not merge with the baseline measured in the blank solution. A small shoulder on Y_F'' at −0.6 V at the highest concentration indicates an overlapping "adsorption prewave" of the Brdička type,[32] which indicates a stronger adsorption of the product, the dimer. Hence the adsorption contribution will contribute to the frequency dependence of Y and has to be taken into account in analysis of data. Adsorption in acetonitrile is evidently present but not too strong because DC polarograms and voltammograms do not yield adsorption prewaves.

Another important feature of AC polarograms is the observation that the imaginary faradaic component Y_F'' is in all cases smaller than the real faradaic component Y_F'. We recall that strongly adsorbing redox couples[33] would yield $Y_F'' \gg Y_F'$, which may lead to a priori nonseparability of charging and faradaic parameters.[34] Because the present system is characterized by $Y_F'' < Y_F'$ and the peak potentials are located slightly more negatively from the polarographic half-wave potentials, it is possible to estimate the heterogeneous rate constant k^0_{Red} provided that the adsorption is properly accounted for.[35]

The separation of the vector of the faradaic admittance (with components Y_F' and Y_F''), the Warburg diffusion impedance, the double-layer capacity C_{dl}, and the adsorption capacity C_a is

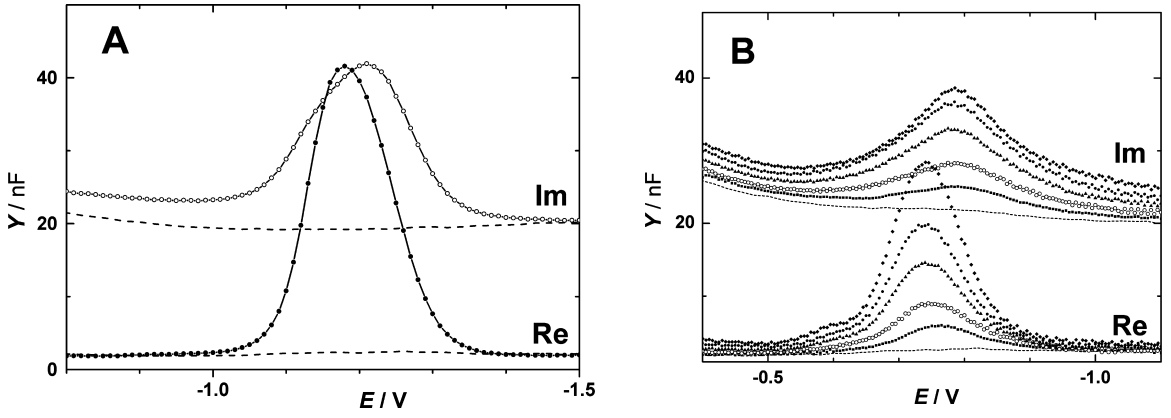

Figure 6. Phase-sensitive AC polarograms of (A) 0.62 mM **1** and (B) **2** in 0.1 M $TBAPF_6$ in acetonitrile. The concentrations of **2** in panel B were 0.053 mM (■), 0.102 mM (◇), 0.212 mM (▼), 0.318 mM (●), and 0.53 mM (◆). Dashed curves correspond to the blank. The superimposed AC signal parameters were 64 Hz and 10 mV amplitude. The imaginary and real admittance components are labeled Im and Re, respectively.

dx.doi.org/10.1021/jp211122n | J. Phys. Chem. C 2012, 116, 3779−3786

based on their different dependence on the applied frequency, ω. Furthermore, the present system will include at low frequencies the impedance originating from the homogeneous dimerization reaction, called the Gerischer impedance.[36] The desired analysis would be best achieved from the EIS measured over a broad range of frequencies. It turned out that the lowest frequency range, <10 Hz, produces useless data. This is caused by the system evolution in time, and the EIS data depend on the direction in which the frequency is varied (low to high or high to low frequencies). This is evidently caused by the dimer adsorption, leading to a self-inhibition, which decreases the electron transfer rate. An illustrative example is given in Supplement 2 in the Supporting Information. For this reason, the frequency scanning by the frequency response analyzer was used only to estimate the solution resistance and the value of $C_{dl} + C_a$ as a function of the applied DC potential (Supplement 4 in the Supporting Information). These values were evaluated in the frequency range where EIS data were time-invariant (70 to 5 kHz).The heterogeneous rate constants were evaluated from impedance vectors recorded on the Hg drop electrode renewed every 1.5 s. Two examples are given in Figure 7; other

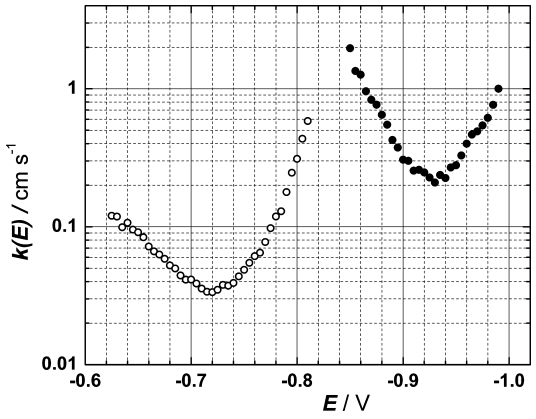

Figure 7. Heterogeneous rate of 0.52 mM **4** (●) and 1.3 mM **2** (○) in 0.1 M $TBAPF_6$ in acetonitrile. Data were evaluated from AC polarograms measured with the sine frequency of 320 Hz. Consistent data were obtained also at 32 and 640 Hz. The time of the Hg drop was 1.5 s.

heterogeneous rate constants of reduction $k^0_{Red,ac}$ are listed in Table 2. The charge transfer coefficient was evaluated from the

Table 2. Kinetic Parameters of the Heterogeneous Reduction and the Homogeneous Dimerization Reactions[a]

compound	$k^0_{Red,ac}$	$k^0_{Red,sim}$	E^0_{Red}	k_{Dim}
1	0.70	0.609	−1.224	1.2×10^6
2	0.033	0.0428	−0.795	4.5×10^6
3	0.038	0.031	−0.730	5.0×10^6
4	0.23		−0.958	

[a]Values of k^0 are in $cm \cdot s^{-1}$, E^0 in V, and k_{Dim} in $M^{-1} \cdot s^{-1}$.

slope of $k(E)$ versus E. The consistency was checked from the dependence of the charge transfer resistance on E obtained from EIS data. The estimated value is $\alpha = 0.62 \pm 0.02$. Diffusion coefficients D were estimated on the basis of the Stokes−Einstein equation relating D and the molecular mass m. Under certain conditions, a linear correlation[37] holds up to $m = 360$, which leads to a value 1.04×10^{-5} cm^2 s^{-1} for **1**. For compounds **2** and **3**, slightly lower values 1.0×10^{-5} and 9.8×10^{-6} cm^2 s^{-1} were calculated. These values were used as an initial estimate for a complete fitting of the cyclic voltammograms, and the results are included in Tables 2 (the reduction and dimerization) and 3 (the dimer oxidation and dissociation).

Table 3. Kinetic Parameters of the Heterogeneous Oxidation of a Dimer and the Homogeneous Dissociation Reactions[a]

compound	$k^0_{Ox,sim}$	E^0_{Ox}	k_{Dis}
1	0.0022	−0.658	4.7×10^6
2	0.0038	−0.083	9.6×10^8
3	0.0064	−0.114	6.0×10^9

[a]Values of k_0 are in $cm \cdot s^{-1}$, E^0 in V, and k_{Dis} in $M^{-1} \cdot s^{-1}$.

The values of $k^0_{Red,ac}$ evaluated from AC data and from simulation of voltammetry $k^0_{Red,sim}$ reasonably agree. An example of experimental data and their numerical fitting is given in Supplement 3 in the Supporting Information.

The absence of the voltammetric oxidation peak of the primary reduction product at high scan rates indicates that the follow-up chemical process is very fast and irreversible. Therefore, the simulation procedures cannot provide a reliable estimate of the equilibrium constants K_{Dim}, which are most likely as high as 10^{10} M^{-1}. The rate constants of dimerization k_{Dim} do not show any significant tendency. However, the rate constants of dissociation of the oxidized dimer k_{Dis} increase by almost two orders of magnitude from one derivative to the next one. This indicates that the stability of $^+$**A-A**$^+$ is very low and substantially decreases from **1** to **3**.

Calculation of the Electronic Structure and Properties. We have concluded that compounds **1**−**3** form dimers upon reduction. To identify possible binding sites for the dimer formation, we inspected respective molecular orbitals and spin densities for the radical species. The LUMO of the parent nonreduced form of the compound **2** is shown in the Supplement 5 in the Supporting Information together with the calculation details. The LUMO coincides with the HOMO of the reduced form. For estimation of the most probable carbon atom, which participates in the bond formation of the dimer, it is important to investigate the spin density distribution of the reduced form. The spin density distribution of the reduced form is shown in Figure 8. Considerably increased spin density is localized on nitrogen atom and on the conjugated carbon atoms in the γ and α positions. It follows from Figure 8 that only the carbon atom in the γ position is available for the formation of a σ-dimer. Similar calculations have been performed for the compound **4**, which does not form a dimer and is reduced reversibly.

The spin density of the reduced form **4** (Figure 9) differs from that of **2**. A significant spin density is localized on nitrogen and sulfur atoms and on the carbon atom connecting N and S atoms. The calculated reduction potentials corresponding to the one electron reduction of the parent cation for all three compounds are in a very good agreement with the experimental estimates: −1.24 (theory) versus −1.22 V (experiment) for **1**, −0.83 versus −0.80 V for **2**, −0.86 versus −0.73 V for **3**, and −0.95 versus −0.96 V for **4**. We were able to optimize dimer structures corresponding to **2**, whereas it was not possible to locate minimum corresponding to **4**. Here we have considered a simplified model of the dimer, considering only the cyclic skeleton common for **1**−**3** without the butyl side chain. The dissociation energy of the dimer **2** was calculated to be 90.7 kJ/mol.

dx.doi.org/10.1021/jp211122n | J. Phys. Chem. C 2012, 116, 3779−3786

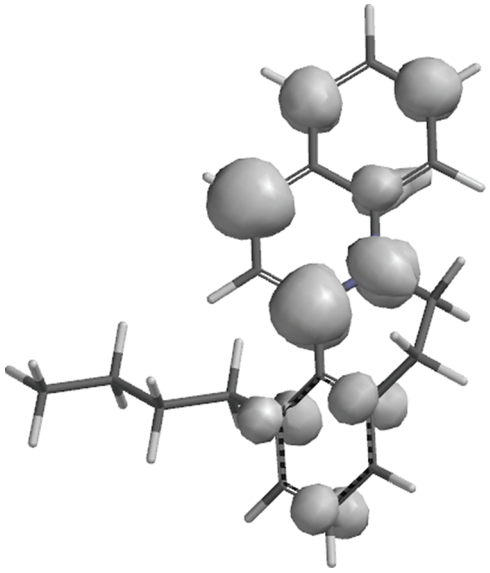

Figure 8. Spin density of the reduced form of **2**.

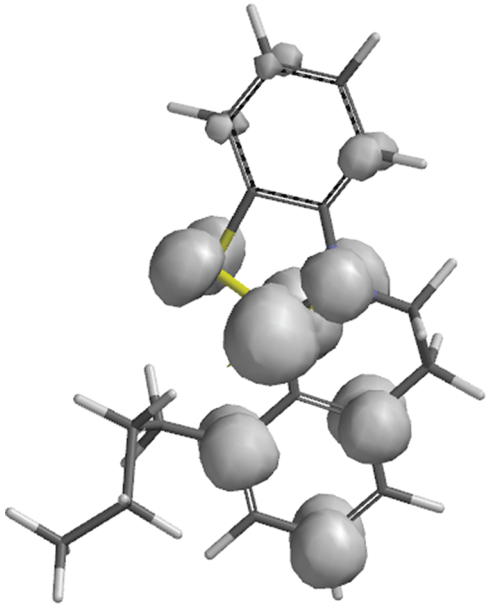

Figure 9. Spin density of the reduced form of **4**.

The neutral dimer (Scheme 2) should therefore be the species that is reoxidized. The oxidation potential for the first electron removal is calculated to be 0.02 V for **2**. The calculated oxidation potential for the second electron transfer is −1.32 V. Experimentally, the oxidation is observed as a single step at about −0.1 V. This suggests that the oxidation is a single step two-electron process with the first electron transfer being the rate-limiting step. Once we remove the second electron, the dimer immediately decomposes into two cations.

Structure of Species Obtained by Reduction. Reduction of cation **4** is straightforward. Upon transfer of charge corresponding to one electron per molecule, the solution color turns red; the resulting sample yields the EPR signal and under an inert atmosphere is stable for several days. Spectroelectrochemical reduction and a subsequent oxidation recover the starting form. The process outlined in Scheme 1 (see eq 5) is consistent with the experimental data collected. The location of

Scheme 1. Reversible Redox-Process for Compound 4

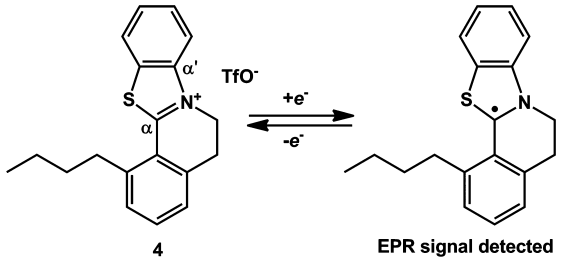

an unpaired electron depicted in Scheme 1 is based on calculated spin density (Figure 9).

The reduction of all three derivatives **1**−**3** yields no EPR signal. The spin density of expected but not detected radicals is calculated to reside on carbon atoms directly connected to the nitrogen atom (i.e., in α positions) and also on the vinylogous position relative to the nitrogen atom (mainly γ-position, Scheme 2 and Figure 8). Calculated spin densities for **2** are

Scheme 2. Proposed Reversible Dimerization Pathway for Compound 2 Yielding Two Possible Diastereoisomers[a]

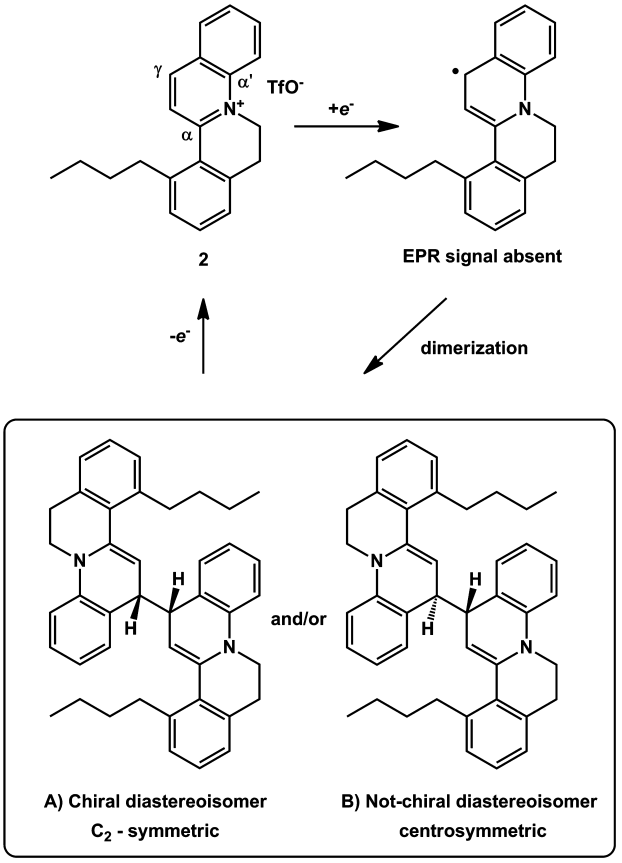

[a]Same mechanism applies also to compounds **1** and **3**.

0.349 and 0.368 for the α- and γ-positions, respectively. The oxidation recovers the starting monocationic form, however, at considerably higher potentials. The calculated structures of radicals show that α positions are sterically hindered, and for this reason the dimerization reaction takes place at the γ position. The dimerization can yield two diastereoisomers, as it is outlined in Scheme 2. An easy oxidation of the resulting dimers leads to a fast regeneration of the original monocationic

dx.doi.org/10.1021/jp211122n | J. Phys. Chem. C 2012, 116, 3779−3786

form (**1**−**3**). The distinction or identification of diastereoisomers of the dimeric species has not been solved in this study.

CONCLUSIONS

We have shown that the investigated pyridinium and quinolinium compounds **1** to **3** are reduced by one electron, yielding radicals that very rapidly form σ dimers. By contrast, in benzothiazolium derivative **4** the electron transfer yields a stable radical in which the follow-up dimerization reaction is completely blocked. Quantum chemical calculations elucidate the role of the charge delocalization for the observed coupled chemical step in species **1**−**3** and its absence in species **4**. The existence of the short-living primary radical generated from **1** to **3** is linked to a significant spin density on the exposed nonsubstituted CH fragment that is in the γ position relative to the nitrogen atom, leading to dimerization.

The analysis of kinetic parameters by simulation of cyclic voltammograms is conveniently facilitated by the estimation of adsorption and heterogeneous electron transfer rates using the AC techniques. The heterogeneous electron transfer rate of **1** is more than one order of magnitude higher as compared with **2** and **3**. The opposite trends were observed for the homogeneous rates of radical dimerization and the dimer dissociation upon electron withdrawal. The estimated redox potentials E^0 for the reduction and the dimer oxidation are quite close for quinolinium compounds **2** and **3**. Pyridinium derivative **1** has considerably lower reduction potential compared with **2** and **3** due to limited delocalization of the smaller aromatic system. The same holds for the dimer oxidation. Only benzothiazolium **4** is reversibly reduced, and its E^0 is directly obtained from experiments. Compounds **1**−**3** can be cycled repeatedly between dimeric and monomeric forms by application of a suitable potential values.

ASSOCIATED CONTENT

Supporting Information

The concentration dependence of AC peak potentials, the complex impedance plot of a time-evolving system, fitting of a cyclic voltammogram by the finite-difference method, analysis of AC polarograms using the low-frequency double-layer capacity, theoretical modeling of structures, LUMO spin density distribution, and UV−vis spectra are given. This material is available free of charge via the Internet at http://pubs.acs.org.

AUTHOR INFORMATION

Corresponding Author

*E-mail: lubomir.pospisil@jh−inst.cas.cz.

ACKNOWLEDGMENTS

This research was supported by the Czech Science Foundation under grants no. 203/09/0705 and 203/09/1614.

REFERENCES

(1) Frey, P. A.; Hegeman, A. D.; Reed, G. H. *Chem. Rev.* **2006**, *106*, 3302−3316.
(2) Halliwell, B. Gutteridge, J. *Free Radicals in Biology and Medicine*, 4th ed.; Oxford University Press: New York, 2007.
(3) *Radicals in Synthesis I: Methods and Mechanisms*, 1st ed.; Gansaeuer, A., Ed.; Topics in Current Chemistry *263*; Springer: New York, 2006.
(4) *Radicals in Organic Synthesis*; Renaud, P., Sibi, M. P., Ed.; VCH: Weinheim, Germany, 2001; Vol. 2.
(5) Dalko, P. I. *Tetrahedron* **1995**, *51*, 7579−7653.
(6) Sibi, M. P.; Manyem, S.; Zimmerman, J. *Chem. Rev.* **2003**, *103*, 3263−3296.
(7) Macías-Ruvalcaba, N. A.; Evans, D. H. *J. Phys. Chem. C* **2007**, *111*, 5805−5811.
(8) Macías-Ruvalcaba, N. A.; Felton, G. A. N.; Evans, D. H. *J. Phys. Chem. C* **2008**, *113*, 338−345.
(9) Macías-Ruvalcaba, N. A.; Evans, D. H. *J. Phys. Chem. C* **2010**, *114*, 1285−1292.
(10) Majranovskij, S. G. *Dokl. Akad. Nauk SSSR* **1956**, *110*, 593.
(11) Koutecký, J.; Hanuš, V. *Collect. Czech. Chem. Commun.* **1955**, *20*, 124.
(12) Gaudiello, J. G.; Larkin, D.; Rawn, J. D.; Bancroft, E. E.; Blount, H. N. *J. Electroanal. Chem.* **1982**, *131*, 203−214.
(13) Olmstead, M. L.; Hamilton, R. G.; Nicholson, R. S. *Anal. Chem.* **1969**, *41*, 260.
(14) Andrieux, C. P.; Nadjo, L.; Savéant, J.-M. *J. Electroanal. Chem.* **1970**, *26*, 147−186.
(15) Macías-Ruvalcaba, N. A.; Telo., J. P.; Evans, D. H. *J. Electroanal. Chem.* **2007**, *600*, 294−302.
(16) Savéant, J.-M. *Acta Chem. Scand.* **1983**, *B37*, 365−378.
(17) Del Sesto, J. S.; Miller, J. S.; Lafuente, P.; Novoa, J. J. *Chem.—Eur. J.* **2002**, *8*, 4894−4908.
(18) Kubo, T.; Katada, Y.; Shimizu, A.; Hirao, Y.; Sato, K.; Takui, T.; Uruichi, M.; Yakushi, K.; Haddon, R. C. *J. Am. Chem. Soc.* **2011**, *133*, 14240−14243.
(19) Rokosha, S. V.; Kochi, J. K. *Acc. Chem. Res.* **2008**, *41*, 641−653.
(20) Korivi, R. P.; Wu, Y.-C.; Cheng, C.-H. *Chem.—Eur. J.* **2009**, *15*, 10727−10731.
(21) Čížková, M.; Kolivoška, V.; Císařová, I.; Šaman, D.; Pospíšil, L.; Teplý, F. *Org. Biomol. Chem.* **2011**, *9*, 450−462.
(22) Adriaenssens, L.; Severa, L.; Šálová, T.; Císařová, I.; Pohl, R.; Šaman, D.; Rocha, S. V.; Finney, N. S.; Pospíšil, L.; Slavíček, P.; Teplý, F. *Chem.—Eur. J.* **2009**, *15*, 1072−1076.
(23) Severa, L.; Adriaenssens, L.; Vávra, J.; Šaman, D.; Císařová, I.; Fiedler, P.; Teplý, F. *Tetrahedron* **2010**, *66*, 3537−3552.
(24) Adriaenssens, L.; Severa, L.; Koval, D.; Císařová, I.; Belmonte, M. M.; Adán, E. C. E.; Novotná, P.; Sázelová, P.; Vávra, J.; Pohl, R.; Šaman, D.; Urbanová, M.; Kašička, V.; Teplý, F. *Chem. Sci.* **2011**, *2*, 2314−2320.
(25) Boese, A. D.; Martin, J. M. L. *J. Chem. Phys.* **2004**, *121*, 3405−3416.
(26) Frisch, M. J.; Trucks, G. W., Schlegel, H. B.; Scuseria, G. E.; Robb, M. A.; Cheeseman, J. R.; Scalmani, G.; Barone, V.; Mennucci, B.; Petersson, G. A.;et al. *Gaussian 09*, revision A.1; Gaussian, Inc.: Wallingford, CT, 2009.
(27) (a) Baik, M.-H.; ad Friesner, R. A. *J. Phys. Chem. A* **2002**, *106*, 7407−7412. (b) Fu, Y.; Liu, L.; Yu, H.-Z.; Wang, Y.-M.; Guo, Q.-X. *J. Am. Chem. Soc.* **2005**, *127*, 7227−7234. (c) Roy, L. E.; Jakubikova, E.; Guthrie, M. G.; Batista, E. R. *J. Phys. Chem. A* **2009**, *113*, 6745−6750.
(28) Tomasi, J.; Mennucci, B.; Cammi, R. *Chem. Rev.* **2005**, *105*, 2999−3093.
(29) (a) Reiss, H.; Heller, A. *J. Phys. Chem.* **1985**, *89*, 4207−4213. (b) Kelly, C. P.; Cramer, C. J.; Truhlar, D. G. *J. Phys. Chem. B* **2007**, *111*, 408−422.
(30) Henry, J. B.; Mount, A. R. *J. Phys. Chem. A* **2009**, *113*, 13023−13028.
(31) Rueda, M.; Compton, R. G.; Alden, J. A.; Prieto, F. *J. Electroanal. Chem.* **1998**, *443*, 227−235.
(32) Brdička, R. *Z. Elektrochem.* **1942**, *48*, 278.
(33) Pospíšil, L. *J. Electroanal. Chem.* **1976**, *74*, 369.
(34) Delahay, P. *J. Phys. Chem.* **1966**, *70*, 2373−2379.
(35) De Levie, R.; Pospíšil, L. *J. Electroanal. Chem.* **1969**, *22*, 277.
(36) Gerischer, H. *Z. Phys. Chem. (Leipzig)* **1951**, *198*, 286.
(37) Valencia, D. P.; González, F. J. *Electrochem. Commun.* **2011**, *13*, 129.